Prediction of Clouds and Rain Using a *z*-Coordinate Nonhydrostatic Model

J. STEPPELER,* H. W. BITZER,+ Z. JANJIC,# U. SCHÄTTLER,* P. PROHL,* U. GJERTSEN,@ L. TORRISI,& J. PARFINIEVICZ,** E. AVGOUSTOGLOU,++ AND U. DAMRATH*

*DWD, Offenbach, Germany
+Aw Geophys, Offenbach, Germany
#NCEP, Camp Springs, Maryland
@met.no, Oslo, Norway
&CNMCA, Rome, Italy
**IMGW, Warsaw, Poland
++HNMS, Athens, Greece

(Manuscript received 2 February 2006, in final form 21 June 2006)

ABSTRACT

The most common option for numerical models of the atmosphere is to use model layers following the surface of the earth, using a terrain-following vertical coordinate. The present paper investigates the forecast of clouds and precipitation using the *z*-coordinate nonhydrostatic version of the Lokalmodell (LM-*z*). This model uses model layers that are parallel to the surface of the sphere and consequently intersect the orography. Physical processes are computed on a special grid, allowing adequate grid spacing even over high mountains. In other respects the model is identical to the nonhydrostatic terrain-following version of the LM, which in a number of European countries is used for operational mesoscale forecasting. The terrain-following version of the LM (LM-tf) is used for comparison with the forecasts of the LM-*z*. Terrain-following coordinates are accurate when the orography is shallow and smooth, while *z*-coordinate models need not satisfy this condition. Because the condition of smooth orography is rarely satisfied in reality, *z*-coordinate models should lead to a better representation of the atmospheric flow near mountains and consequently to a better representation of fog, low stratus, and precipitation. A number of real-data cases, computed with a grid spacing of 7 and 14 km, are investigated. A total of 39 real-data cases have been used to evaluate forecast scores. A rather systematic improvement of precipitation forecasts resulted in a substantial increase of threat scores. Furthermore, RMS verification against radiosondes showed an improvement of the 24-h forecast, both for wind and temperature. To investigate the possibility of flow separation at mountain tops, the flow in the lee of southern Italy was investigated.

1. Introduction

It has long been known that, generally, the atmosphere at rest cannot be represented properly in atmospheric models using a terrain-following coordinate system. Sundqvist (1976) used a global model with initial values corresponding to horizontally homogeneous temperature and mass fields in hydrostatic balance. Although the atmosphere should have remained at rest with these initial values he found velocities of several meters per second in the vicinity of mountains. The reason is the error made in the computation of the horizontal component of the pressure gradient force, which is computed using derivatives along the model coordinate surfaces and in the vertical (e.g., Janjic 1977). While no tests for cases with large velocities have been reported in the literature, the error may be expected to be large, because the computation of the advection will also be wrong. The numerical approximations used with terrain-following coordinates are accurate only for gently sloping mountains. For better accuracy, it is required that $dh < dz$, where dh is the change of orographic height from one grid point to the next, and dz is the vertical grid interval. This condition can be satisfied in idealized tests using bell-shaped mountains, such as done by Saito et al. (1998) or Gallus and Klemp (2000). With real topography, however, this condition is often violated, and numerical errors occur near mountains that appear as mountain-generated artificial forcing. It is easier to neglect this error in large-

Corresponding author address: J. Steppeler, Deutscher Wetterdienst, Kaiserlaistr. 42, 63067 Offenbach, Germany.
E-mail: juergen.steppeler@dwd.de

scale models with grid spacings of hundreds of kilometers, because it affects the mesoscale flow near mountains, which has only an indirect effect on the prediction of large-scale features, such as the movement of synoptic-scale highs and lows.

In mesoscale models with a grid spacing of several kilometers, however, the mountain-generated mesoscale flows are of direct concern, because these are the forecast features of interest. In particular, errors in the mountain-generated circulation can have a direct impact on mesoscale cloud structures and local precipitation. In this paper, a version of the Lokalmodell (LM; Steppeler et al. 2002b), the the z-coordinate nonhydrostatic LM (LM-z), is used to investigate the impact of z-level vertical discretization on mesoscale prediction.

The terrain-following version of the model, denoted here as LM-tf, is used operationally at a grid spacing of 7 km with 35 layers. It almost systematically fails to forecast low stratus north of the Alps (Ch. Schraff, DWD, 2002, personal communication), mainly in low wind situations. Quantitative precipitation forecasting is still an outstanding problem for mesoscale models. Forecasters using the LM consider this an area where progress would be most welcome (Papageorgeou, HNMS, 2003, personal communication). Currently there is a joint effort by German universities sponsored by the German Research Council (DFG; grant SPP1167) to improve the precipitation forecasts of the LM and other models. A list of acronyms is given in Table1. The errors present in the current LM concern the distribution of precipitation and have a systematic component, such as frequent overprediction of maxima. This latter error has been reduced with recent model changes (introduction of prognostic precipitation and orographic smoothing), but is still a problem.

Models using a discretization in the z coordinate are able to represent the atmosphere at rest exactly and avoid the errors due to sloping coordinate surfaces. A technique based on step-mountain representation in the z coordinate was originally proposed by Bryan (1969), and subsequently widely used in oceanography. Mesinger et al. (1988) applied the step-mountain blocking in a pressure sigma coordinate model [the National Centers for Environmental Prediction (NCEP) Eta Model]. This approach assumes the mountains are represented by piecewise constant functions and internal boundary conditions are needed at the vertical walls. This step orography is also known as brick (or Lego) approach, as the orography appears as being created by bricks, with only vertical and horizontal surfaces occurring. Mathematically, the function used for the approximation of the mountains is said to be of type c0. This means that the orographic function has jumps at the interfaces of grid boxes. Functions of type c1 are those represented by bilinear splines, when the function has no jumps at the interfaces of grid volumes. It can be shown that a sufficient condition for convergence of the solution can be derived when the lower boundary function is approximated by a c1 function (see Kröner 1997).

TABLE 1. List of acronyms.

ARPA	Regional Meteorological Center of Bologna, Italy
Aw Geophys	Military Meteorological Service of Germany
COSMO	Consortium for Small-Scale Modeling: Association of the weather services of Switzerland, Italy, Poland, Romania, Greece, and Germany for the further development of the LM
DFG	German Research Council
DWD	German Meteorological Center
IMGW	Meteorological Center of Poland
HNMS	Greek Meteorological Center
CNMCA	Meteorological Center of Italy, Rome, Italy

For c0 boundary functions no similar result could be obtained. The NCEP Eta Model using the step-mountain approach worked well on the synoptic scales, but difficulties have been encountered on the mesoscales. Although the atmosphere at rest can be represented very accurately using the step mountains, it was shown by Gallus and Klemp (2000) and by Gallus (2000) that there are serious problems with this approach on the mesoscale in the presence of wind. Gallus and Klemp used a shallow mountain of 400-m height, which was well resolved by grid points. In contrast to the step mountains, the terrain-following coordinate gives good solutions in this situation. It was shown that the linear gravitational wave was well represented with the terrain-following coordinate, but seriously misrepresented with the step mountains. There were two types of errors identified by Gallus and Klemp (2000). The first error results in a distortion of the vertical velocities of the classic mountain wave pattern with disturbances directly over the corners of the mountain steps. The second error consists of spurious flow separation at mountain tops, which leads to artificial wind sheltering behind mountains. The second problem may be potentially more serious, because Gallus and Klemp (2000) report that it does not decrease when the vertical grid spacing is substantially reduced. This is a practical consequence of the lack of convergence. In the operational applications of the Eta Model in Greece (G. Sakellaridis, HNMS, 2000, personal communication) and Italy (T. Paccagnella, ARPA, 2002, personal communication) a strong underestimation of winds in the lee sides

of mountains was observed (see also Staudenmaier and Mittelstadt 1997). The operational applications in these two countries changed to the terrain-following model LM after 2000. Because gravitational waves generated by mountains play a role in the mesoscale precipitation mechanism, these deficiencies of the step approach are important, when forecast models go toward higher grid spacing. According to F. Mesinger (NCEP, 2004, personal communication) an alternative formulation of the bottom boundary of the Eta Model has been developed, taking account of the slope of the boundary. With this alternative boundary treatment the problems mentioned above do no longer occur.

A different concept for the z coordinate is that by G. Tripoli (2001, personal communication; see Saito et al. 2001). This approach uses the vorticity field to obtain boundary values at the orographic surface. It avoids the problems mentioned above.

The z-coordinate modeling used in this study is based on approximating the orography by a c1 function, being a piecewise bilinear function that is continuous at the intersections of grid volumes. The method is described by Steppeler et al. (2002a) for a dry two-dimensional model. This approach is free from the problems pointed out by Gallus and Klemp (2000). Simple tests of this method using the dry model were performed in Steppeler et al. (2002a). The intention of the present paper is to investigate the impact of the z discretization on numerical forecasts in more realistic situations. Section 2 describes how the model investigated in Steppeler et al. (2002a) is converted into the LM-z model, which is suitable for real-data weather forecasts. Some further idealized integrations involving physical processes are presented in section 3. Section 4 presents cases starting from real initial values using the LM-z. The results are compared with those of the LM-tf. To investigate the implication for quantitative precipitation forecasts and mesoscale circulations, 39 cases from three different model areas are used to compute scores. As spurious flow separation and associated underprediction of wind in the lee of mountains was a problem in Eta Model predictions, the flow in the lee of the southernmost tip of Italy was investigated.

2. The LM-z forecast model

The LM-z model was designed to use the z discretization, and to be identical to the model described in Steppeler et al. (2002b) in all other respects. The discretization on z coordinates is described in Steppeler et al. (2002a). Starting from this, the following developments had to be completed in order to obtain a model suitable for forecasts using real initial data:

- The introduction of the prognostic moisture fields (specific humidities): water vapor q, liquid water qc, and cloud ice qi.
- The generalization of the code to three dimensions.
- The parameterization of physical processes: cloud microphysics, boundary layer turbulence, radiation, surface processes, and moist convection.
- The creation of an interface to obtain realistic initial and boundary values.

The advection of moisture variables was done in the same way as described by Steppeler et al. (2002a) for the advection of temperature.

The generalization of the code to three dimensions poses no difficulty in principle, although it involves a lot of technical work. Figure 1 (left) illustrates the representation of the orographic function in three space dimensions by a bilinear function. The discretization volumes are defined as the intersection of regular grid cells with this bilinear spline. There are cells completely above or below the orographic function and those partially above orography. As with two dimensions, weights have to be associated with the surfaces of the discretization volume. Each such surface is intersected by the bilinear orographic function as a straight line. The weight associated with this surface is the ratio of the area on the side of this line being in the atmosphere to the full area of the surface.

The parameterization of the physical processes is done using the parameterization package of the LM-tf, as described by Steppeler et al. (2002b). Because the LM-tf works on terrain-following coordinate surfaces, this terrain-following grid is introduced as a second grid. For each field f there exist now two representations, corresponding to representations on the two grids, f^z and f^p. The terrain-following grid is called the physics grid, as it is only used to compute the contributions of the physical processes. The physics package of the LM-tf allows any distribution of levels to be used, as long as there is the same number of levels above every horizontal point. For simplicity in this paper the levels are chosen as used operationally with the LM-tf. The two systems of model layers are also shown in Fig. 1 (right). Transformations I are defined to transform between these two representations:

$$f^p = If^z$$
$$f^z = I^{-1}f^p. \tag{1}$$

It should be noticed that these transformations must be defined so that they do not use gridpoint values under a mountain. Thus, the values at these underground points can take on any value, without affecting the fore-

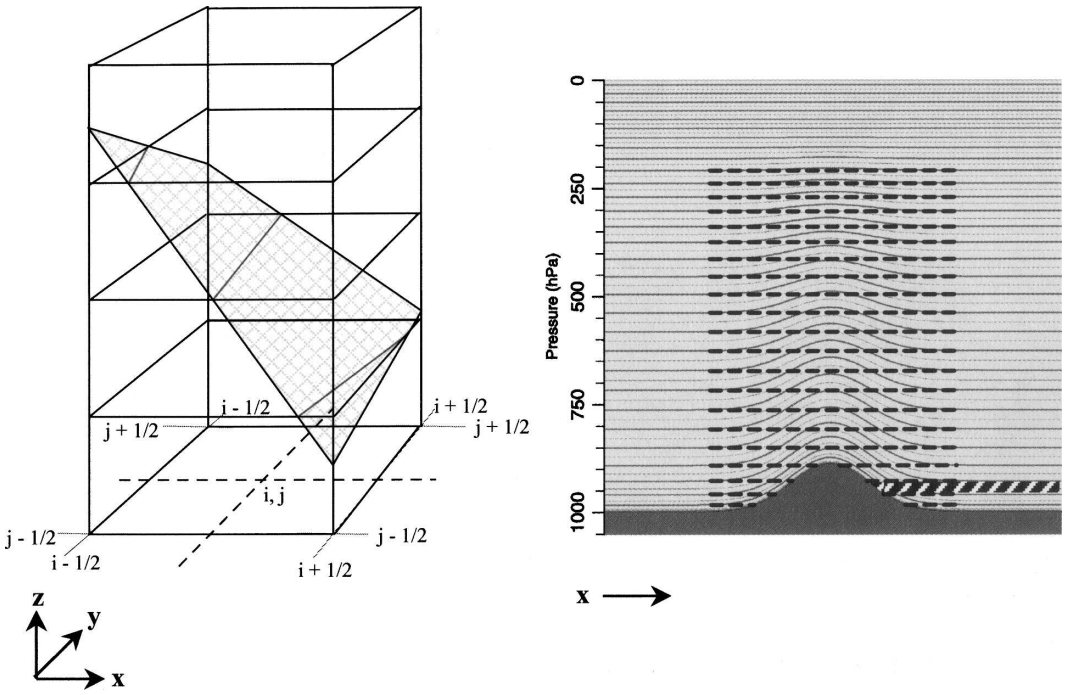

FIG. 1. Representation of the orographic function for the three-dimensional model by a piecewise bilinear function. (left) The column belonging to grid point i, j. The orographic values are defined at the edges of the column, at indices $i + 1/2, j + 1/2$; $i - 1/2, j + 1/2$; $i - 1/2, j - 1/2$; $i + 1/2, j - 1/2$. The cubes indicated by the solid lines are the computational volumes belonging to the horizontal index i, j. The shaded surface is the bilinear surface defined by the orography on the edges of the column. The atmospheric part of a computational volume is that above this bilinear surface, and the part below it is inside the mountain. (right) A cross section showing the terrain-following model levels as solid lines. All model fields, except vertical velocity w, are defined on these lines. The thin dotted lines are the half levels. It may be assumed that the field amplitudes define a field between two half levels. In the LM-z, the terrain-following grid is used to compute the physics tendencies. The z grid is indicated by dashed lines, and model surfaces may disappear under the mountain. The shaded area indicates a model layer for the vertical velocity field w, which is defined on the half levels. The vertical axis is the pressure of a standard atmosphere, having 1000 hPa as surface pressure.

cast at the points in the free atmosphere above the mountain. The transformation is in the same way valid for time derivatives defined on the two grids. Above mountains, the physics grid can have increased grid spacing compared with the z grid (see Fig. 1). Therefore the two transformations cannot be inverse to each other, as they transform between spaces of different dimensions.

The dynamics and physics processes of LM-z are computed each only once per grid point, though on different grids. The small computational overhead is only the computation of the operators I and I^{-1}. Therefore the computational cost per grid point and time step is the same for LM-tf and LM-z. The storage requirement, however, is about double for the LM-z. As an example, the LM-tf runs in the "Europe configuration" using $665 \times 657 \times 40$ points on 528 IBM power 5 processors. It uses 100 mb on each processor.

For the work reported in this paper cubic spline interpolation was used to define the operators I and I^{-1}. This option is most easily implemented, as an arbitrary choice for the physics grid can be used. Therefore it is possible to employ the grid used in the operational LM-tf to compute the physics tendencies. A disadvantage of this approach is the interpolation error, which is accumulated every time step. However, it is possible to eliminate this error. In fact, by choosing the grids such that the z grid is a subgrid of the physics grid, it is possible to define the transformations I and I^{-1} to have the mathematical properties of a projection ($I = I^{-1}$, $II = I$), which implies that the formalism to be described below will avoid this error. This concept, which may be interesting for future versions of the scheme, is discussed in the appendix.

Let g now stand for vertical grid representations of the model fields, which are the three velocity components, pressure, temperature, and specific humidities for water vapor, cloud water, and cloud ice. Let $P(g^p)$ then be the time derivatives as computed by the physics routines on the physics grid. In the following, the upper

index of a field will indicate the grid in which it is represented; that is, it will be either z or p. For time derivatives also a lower index is used. It indicates the process, to which this time derivative belongs, either the physical processes indicated by p, or the adiabatic processes indicated by z. Because the physics routines compute the physics tendencies on the physics grid, we may write

$$(\partial g/\partial t)_p^p = P(g^p).$$

The simplest way to define time derivatives due to the physics on the z grid is then:

$$(\partial g/\partial t)_p^z = I^{-1}P(Ig^z). \quad (2)$$

The time derivatives corresponding to the physics tendencies given above in the z grid can be used in the normal way to add the physics time step increment on the z grid by an Euler time step. However, above high mountains the physics grid is typically much finer than the z grid, and therefore fine boundary layer structures would be lost with the z grid. An alternative approach described below avoids this disadvantage.

The z-grid values are created from the physics grid at the initial time. This has the additional advantage that the LM-z can start from the same initial files as the LM-tf:

$$g^z = Ig^p. \quad (3)$$

Then the dynamics are computed on the z grid and the physics package is run on the physics grid. Then physics tendencies are computed on the z grid and adiabatic tendencies on the physics grid:

$$\begin{aligned}(\partial g/\partial t)_p^z &= I^{-1}(\partial g/\partial t)_p^p \\ (\partial g/\partial t)_z^p &= I^{-1}(\partial g/\partial t)_z^z. \end{aligned} \quad (4)$$

The dynamics and physics tendencies are both defined on each grid, and time step is performed on each of these grids, using both the z-grid and the p-grid tendencies. This method is able to create and preserve realistic boundary layer structures even over mountains, where the z grid is too coarse to represent the boundary layer properly. These vertically well resolved fields are then used in the subsequent physics calculations. They are able to compute fluxes for the boundary layer scheme, which are not inferior to those of the LM-tf, as they do not suffer from reduced grid spacing. The part of the physics tendencies corresponding to the coarser resolved z levels is made available to the fields in z representation by interpolation. While the scheme given in Eq. (2) can be considered to be a quick method to obtain a physical parameterization in the LM-z, the scheme described by Eq. (4) may have merits beyond this. It uses a process-related grid in order to compute the physical package on a finer grid spacing than the dynamic tendencies, which are computed on the z grid. Both dynamics and physics are thus computed on a dedicated grid well suited for the particular process.

In an attempt to implement the finite-volume concept as closely as possible, rather small cutoff volumes were admitted in the LM-z. These small elements require a small time step, being one-quarter of that used operationally. The control runs were performed using the same reduced time step. The operational time step can be used when artificially enlarging the computational volumes in terms concerning the fast waves (Steppeler et al. 2002a). As we want to investigate the finite-volume z discretization with no additional assumptions in this study, this approximation was not made, though it will be important for an eventual operational application of LM-z.

The z discretization involves in particular the computation of the fourth-order horizontal diffusion operator on z surfaces, where at mountain surfaces boundary conditions are used. A similar approach for the diffusion terms was used by Zängl (2002) when treating the other dynamic terms in terrain-following coordinates. An improvement of wind forecasts was found with this partial transition to the z approach.

Orographic filtering is necessary with LM-tf in order to obtain good precipitation forecasts (Steppeler et al. 2002b). With LM-z, orographic filtering is not necessary. In section 4 an example of the two orographies used with LM-z and LM-tf will be shown in a cross section. Such differences in orographic heights are known to have a considerable impact on forecast skill (Wallace et al. 1983).

V-shaped valleys are defined by only one grid point. They are potentially a bigger problem with LM-z, as neither advection nor horizontal diffusion provide an exchange with neighboring grid points. LM-tf always provides horizontal exchange, but still occasionally has problems in such situations. It would be no problem to create a z discretization, which in such situations becomes one dimensional, retaining only the physical processes acting in the vertical. As the LM physics does not act very well in long-term one-dimensional integrations, v-shaped valleys were filled for the LM-z integrations. This filling of v-shaped valleys was not used with LM-tf. In all other respects the options used for the control run were the same for the two model integrations. In particular the reduced time steps used with LM-z were in the same way used with LM-tf. The thin wall approximation was proposed in Steppeler et al. (2002a) to achieve the normal time steps used with LM-tf operationally. It was tested in one realistic case to show that the LM-z runs stable with the enlarged time step. It was not used for the systematic model compari-

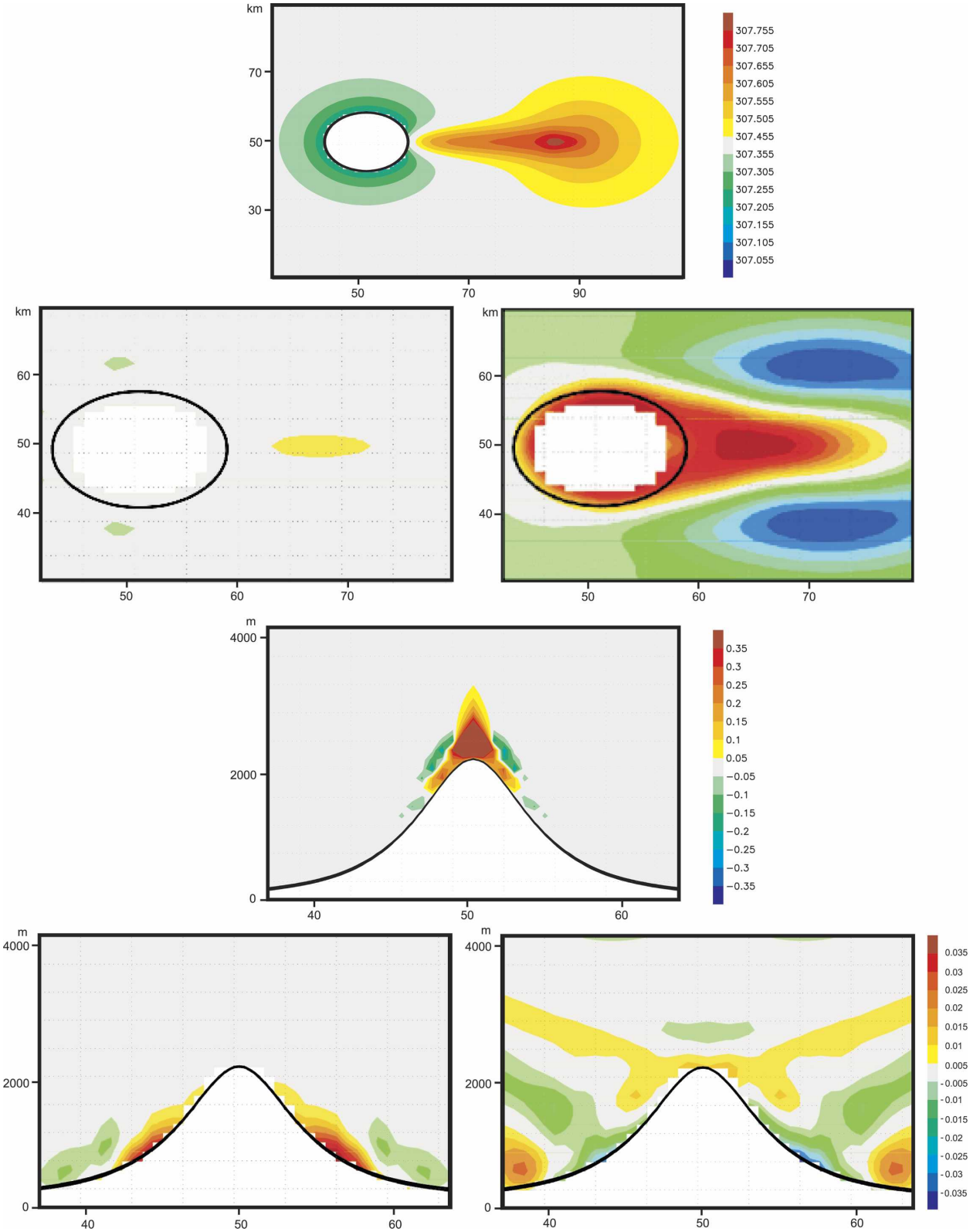

FIG. 2. Flow around a bell-shaped mountain (2-h forecasts). (top) Forecast of the LM-tf with radiation switched off. The temperature field in kelvin is shown for a horizontal cross section at height 150 m for the flow around a mountain of height 400 m. The labels of the *x* and *y* axes are grid point numbers in a 2-km grid. (second row from top, left) As in top, but for LM-*z*. Please note the different

son, as it is an additional approximation that should be tested separately.

3. Idealized tests

The first tests were performed using a bell-shaped mountain of 400-m height with initial values representing a homogeneous wind field of 10 m s^{-1} blowing from the west. The temperature field is horizontally homogeneous and represents a stable atmosphere. It is the same temperature profile used for the two-dimensional tests in Steppeler et al. (2002a). The run without physical parameterization using LM-*z* has very much a two-dimensional character for the lower levels. Figure 2 (second row, left) shows the temperature in a horizontal cross section at height 150 m. This field is homogeneous to a good approximation. This is compared with the result when the dry physics package was switched on, consisting of radiation, boundary layer turbulence, and surface processes. As the run was done during daytime conditions, the mountain surface is heated. This results in an increase of temperature in the wake of the flow. The heating generates a circulation perpendicular to the main axis of the flow, which results in patches of decreased temperature. These results appear to be physically realistic, though no analytic solution for this case exists. For comparison, the result without physics using LM-tf is also shown in Fig. 2 (top). The temperature changes are of the same order of magnitude as produced by the physics and do not seem plausible.

The same test was performed for an atmosphere at rest using a 2300-m-height mountain. The atmosphere remains at rest without physical parameterization, in accordance with the design of the *z*-coordinate discretization. For the case with physics, the vertical velocity in meters per second for a cross section through the center of the mountain is shown in Fig. 2. The results of a 2-h forecast for daytime (bottom left) and nighttime (bottom right) conditions are shown. The model produces mountain and valley winds, as expected in such situations (Pielke and Segal 1986). Figure 2 (third row) also shows the corresponding result for the atmosphere at rest with LM-tf and no radiation. The error is an order of magnitude larger then the velocities obtained by radiation. When comparing to similar results reported in the literature it should be taken into account that the effect depends not only on the geometry of the grid and the mountain, but also on the reference profile. Most nonhydrostatic models use such a reference profile in order to reduce the errors associated with the terrain-following coordinate.

4. Real-data forecasts and the improvement of the quantitative precipitation forecast (QPF) due to LM-*z*

For the real-data calculations, moisture fields are introduced in addition to the dry physics, and treated in the same way as described for temperature in Steppeler et al. (2002a). The moisture fields used as prognostic variables are water vapor, cloud water, and cloud ice. The LM-*z* and the LM-tf are based on older versions of the LM, which treat the precipitation diagnostically, the diagnostic equation for the precipitation phases being obtained by putting the time derivative of the precipitation phases in the Kessler scheme to zero. A prognostic precipitation scheme has since been introduced for the LM, which has substantially improved the forecast of the maxima. These maxima have been very much overpredicted by the older diagnostic scheme. Examples of this overprediction of maxima were given in Steppeler et al. (2002b), where it is shown that the error reached 100 mm in a 24-h interval in some places. Because this improvement is not included in LM-*z* and LM-tr, as they were used here, substantial overprediction of precipitation maxima over mountains can be expected.

Forecasts using realistic initial data were done for 39 cases. The different model areas used are shown in Fig. 3 and are referred to as Warsaw (Poland), Athens (Greece), and Rome (Italy) model areas. One case with initial date 0000 UTC 28 March 1997 used the Warsaw model area (frame 1 in Fig. 3) and a grid spacing of 14 km. This area is somewhat smaller than that used operationally in Warsaw. For this case high-resolution climatological precipitation data were available. As these give the precipitation sums from 0600 UTC to 0600 UTC the following day, this forecast was extended to 30 h. Three cases were done using the Athens model area (frame 2 in Fig. 3) with a grid length of 14 km and starting dates 0000 UTC 6–8 March 2005. Thirty-five

←

horizontal scale compared with the diagram above. (second row from top, right) As in left, but with radiation, corresponding to daytime conditions. (third row from top) Vertical cross section of the vertical wind field in m s^{-1}, 2-h forecast by LM-tf with radiation switched off. The initial values represent an atmosphere at rest, and mountain height is 2300 m. The analytic solution for this case is the atmosphere at rest. (bottom right) As above, using LM-*z* including radiation for nighttime conditions. The horizontal and vertical indices are gridpoint numbers, corresponding to horizontal grid length of 2 km, and the vertical coordinate is height in meters. Please note that the orographic mask shown is only accurate by half a grid length. (bottom left) As in bottom right, but for daytime conditions.

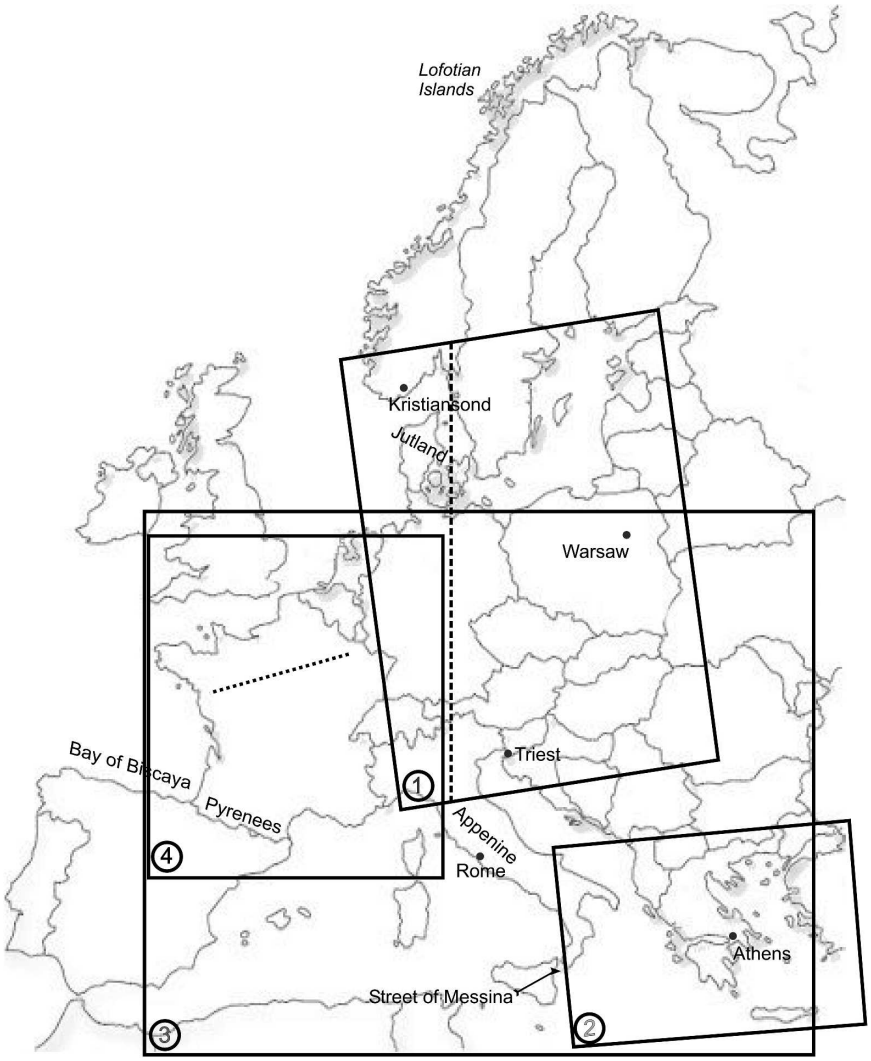

FIG. 3. The model areas used and the orographic locations mentioned in the text: 1: Warsaw model area; 2: Athens model area; 3: Rome model area; 4: Area for output for the frontal rain shown in Fig. 10. The dashed line is for the cross section for the Warsaw case, and the dotted line is for the time–height diagram shown in Fig. 9.

cases of the Rome version (frame 3 in Fig. 3) with a grid spacing of 7 km were done. The initial dates were 0000 UTC 24–29 March 2005 and 0000 UTC 24 April–23 May 2005.

The threat score (2-mm threshold) of the 0600–0600 UTC forecast with the Warsaw model version was 0.58 for the LM-z forecast, as compared with 0.51 for the LM-tf. The scores of 24-h predictions for the three Athens cases are higher for the LM-z (0.40, 0.74, 0.47) as compared with the LM-tf (0.13, 0.57, 0.31). Figure 4 shows threat scores and frequency bias for the 35 cases with the Rome version of LM, together with verifications of 10-m winds and 2-m temperatures. The threat scores for LM-z are substantially higher. The frequency bias for the LM-z is less time dependent and better (closer to 1). The verification of the 10-m winds is about equal between the two model versions. The 2-m temperature verifies much better with LM-z.

RMS verifications against radiosondes of 24-h wind and temperature forecasts are shown in Fig. 5. A rather strong improvement can be seen with the LM-z. It should be kept in mind that this is only a first test. Developments that are important for an eventual operational application are not yet tested extensively, such as the thin wall approximation to achieve large time steps and an improved physics interface using the newest physics cycle.

These rather strong improvements were obtained using a rather old version of the LM physics scheme, dating from April 2002. The latest version of the LM

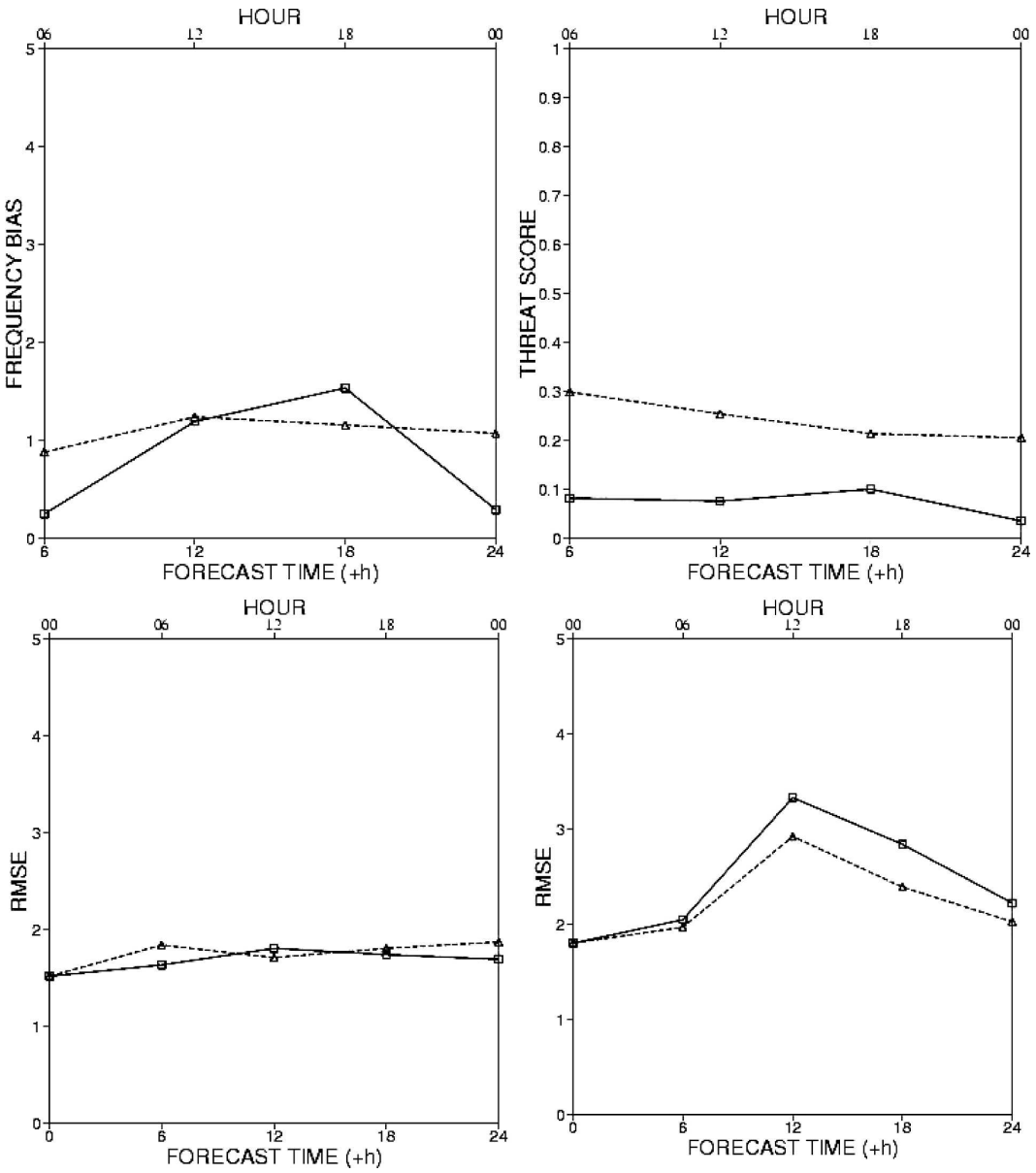

FIG. 4. Forecast scores for 35 cases using the Rome model version. Initial dates 0000 UTC 25 Mar to 0000 UTC 29 Mar 2005 and 0000 UTC 24 Apr to 0000 UTC 23 May 2005. (top left) Frequency bias for 6-h accumulated precipitation as function of forecast time for LM-tf (solid) and LM-*z* (dashed). (top right) As for top left, but for threat score with level 2 mm. (bottom left) RMSE ($m\ s^{-1}$) for 10-m wind speed verification against SYNOP observations as function of forecast time for forecasts with LM-tf (solid) and LM-*z* (dashed). (bottom right) As in bottom left, but for 2-m temperature verification (°C)

physics is not available with LM-*z*. It may be asked if the same improvements can be expected using the new physics. The most important theoretical development in the physics scheme since then was the introduction of prognostic precipitation, which had a rather positive impact on precipitation forecasts. The impact of this change was smaller than that of the transition to LM-*z*. The average increase of forecast scores in a month of predictions was about 5% and visual inspection mainly showed shifts of precipitation patterns of about 50 km, while LM-*z* has an impact on larger-scale precipitation patterns. On the other hand, changes of the parameters used in the physics have a large impact on precipitation amount. One of the cases using the Rome model area (0000 UTC 29 March 2005) was run using LM-tf with the newest model cycle and visual inspection revealed an improvement as rain was produced in areas that were falsely dry with the old version of LM-tf. How-

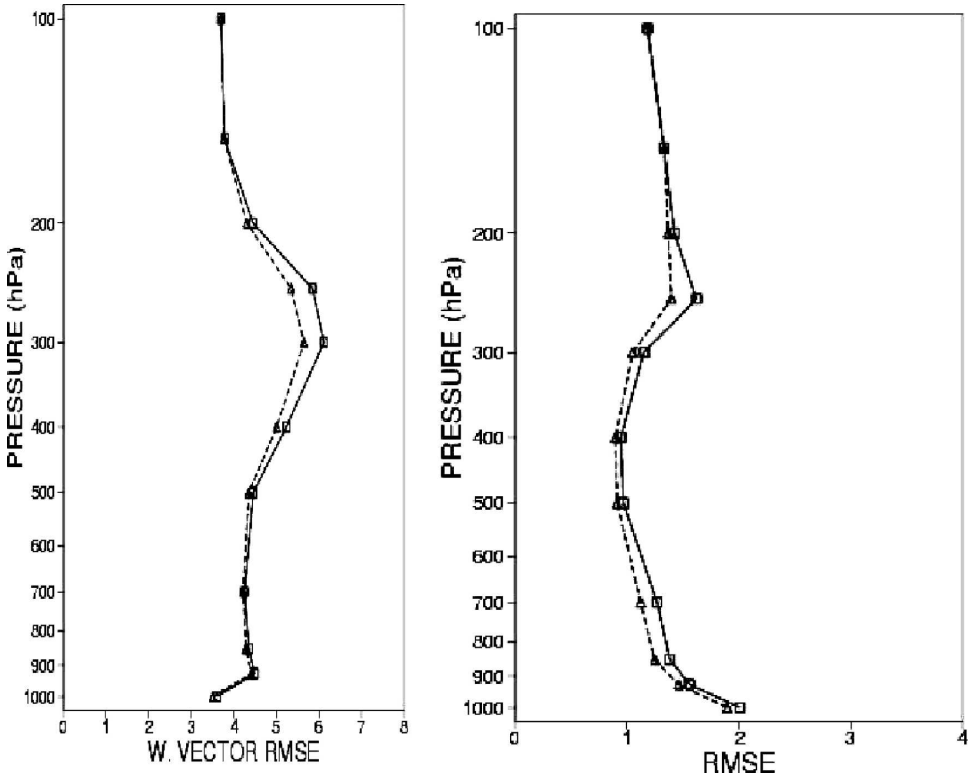

FIG. 5. Radiosonde verifications for the cases used in Fig. 4. (left) RMSE of 24-h vector wind forecasts ($m\ s^{-1}$) for LM-tf (solid) and LM-z (dashed) as function of height (defined by hydrostatic pressure against radiosondes). (right) As in left, but for temperature (°C).

ever, in areas where the rain was already too strong it increased further. For this particular date the improvement of the threat score of the LM-z when using the old physics as compared with the LM-tf using the newest physics cycle went down to 5% on average.

It is possible that the improvement of LM-z compared with LM-tf becomes smaller when the newest cycle of physics will be used. The comparison reported here benefited from the fact that the LM-tf model, providing the control run, was in operational use for only 2.5 yr and therefore only a limited amount of tuning was done. The comparison might have been even stronger in favor of LM-z, if the first version of LM-tf had been used for comparison, which showed rather strong faults in areas of steep topography (Steppeler et al. 2002b). For example in certain Alpine valleys there was no rain in the first year of operations. This particular error was reduced with the introduction of orographic filtering. The LM-z does not need such filtering, as the effect of orography is introduced by the boundary condition and not through terms in the dynamic equations. When considering practical applications of the LM-z for forecasting, it may be considered to retune the physics scheme when using the new LM-z dynamics. The examples discussed in the following indicate that strong differences in forecasted vertical velocity are responsible for the differences in precipitation of the two model versions.

As an example for the changes in the forecast of precipitation produced by the transition to LM-z, the forecast starting from the 0000 UTC 28 March 1997 in the Warsaw model area (frame 1 in Fig. 3) is considered. The meteorological situation involves a small low, which at 1200 UTC is located over Poland. Figure 6 shows the observed precipitation from Germany, Switzerland, and Poland using the relatively dense climatological network, which reports at 0600 UTC. These observations correspond to the predicted accumulated precipitation from 6 to 30 h, also shown in Fig. 6. The precipitation maxima in both forecasts are higher than the observations by a factor of about 2, a well-known error of the LM (see section 1). Both forecasts are missing the precipitation in northwest Poland near the Baltic coast. However, there are interesting differences in the forecast of the mesoscale precipitation structures.

For a number of these structures the LM-z performs better than the LM-tf. Most obvious is the large area of precipitation over northern Germany, to the north west of the city of Hamburg. The LM-tf gives only one maximum, whereas the area of precipitation is much more

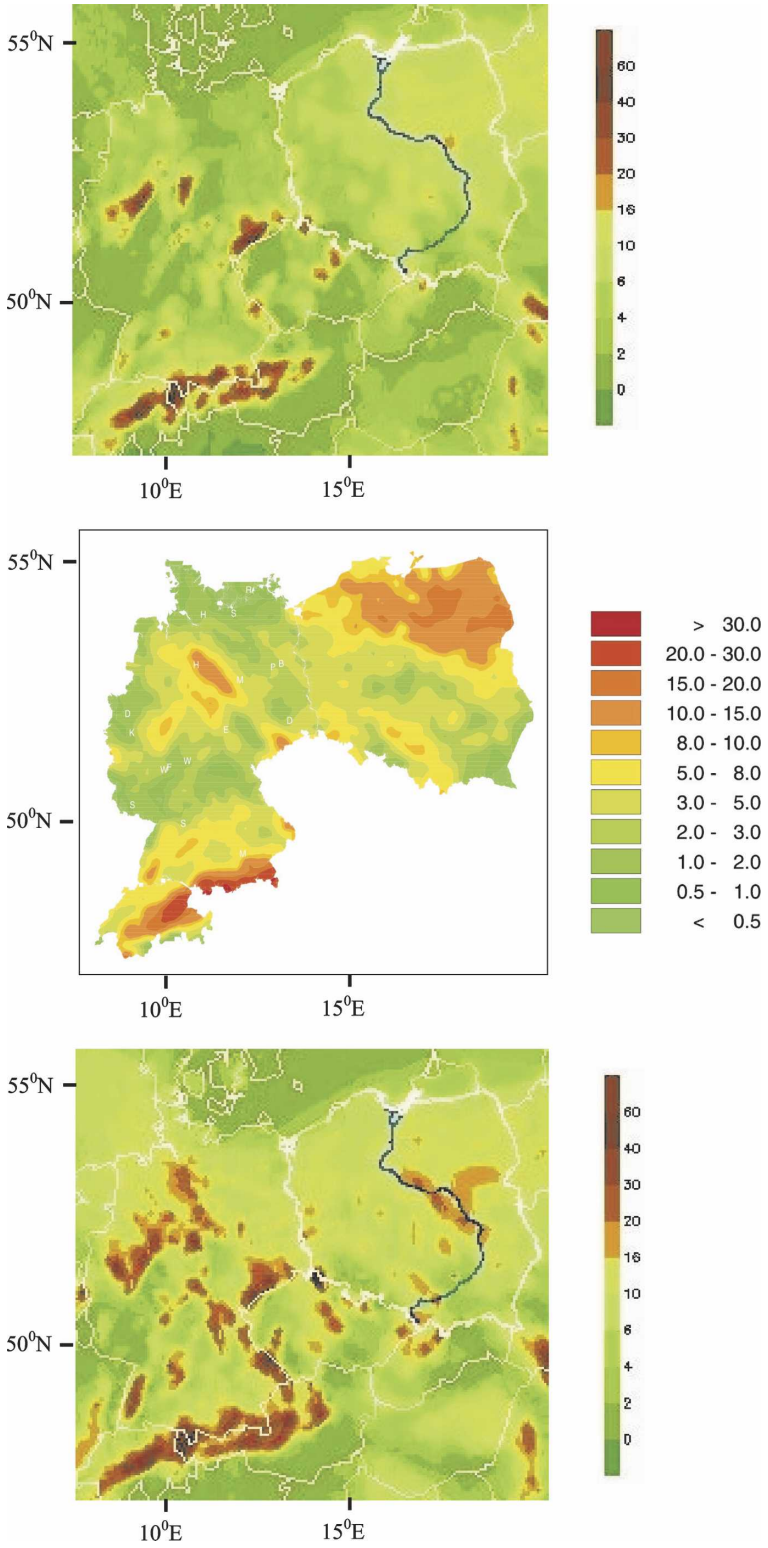

FIG. 6. Forecasted and observed precipitation for 0600 UTC 29 Mar–0600 UTC 28 Mar 1997. (top) The precipitation sum (mm) as forecasted by LM-tf. (middle) The precipitation sum as observed by the climatological gauge network. Data from Germany, Switzerland, and Poland were used. (bottom) As in top but for LM-*z*.

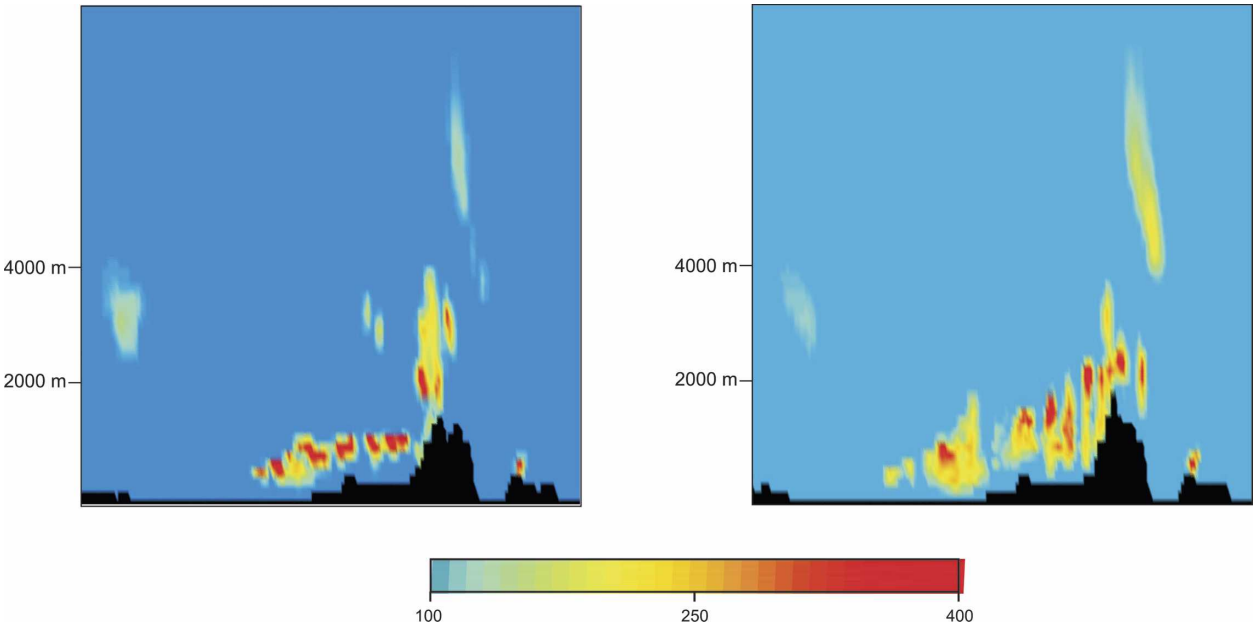

FIG. 7. Forecasted cross sections for cloud water mixing ratio q (mg kg^{-1}) on a line indicated in Fig. 3: (left) 12-h forecast with LM-tf; (right) as in left, but for LM-z.

extended with LM-z. The precipitation at the border between Germany and the Czech Republic is predicted with the LM-z to have a maximum at the southern end of this border, which is in good agreement with observations. The LM-tf locates this maximum more to the north. Over Poland, the LM-tf forecasts very little rain, while the LM-z gives an indication of the extended rain area observed in the east. Also, the observed rainband extending into Poland from the southeast corner of the border between Poland and the Czech Republic is indicated in the LM-z forecast and not in that of the LM-tf. The small spots of precipitation predicted by the LM-z at the border between Germany and Poland are supported by observations.

To see the differences in cloud structure causing these differences, Fig. 7 gives cross sections of the cloud water field in north–south direction on the line indicated in Fig. 3. The differences in orography between LM-z and LM-tf are caused by the orographic filtering, being used with LM-tf but not with LM-z and the filling of v-shaped valleys, being only used with LM-z, as described in section 2. For this particular cross section the difference in orographic height between the two model versions reaches several hundred meters. According to Wallace et al. (1983) such difference in orographic height may be expected to have a relevant impact on the forecast. The cloud cells in the cross section are quite different for the two forecasts. With LM-z they reach higher and are more separated by areas with no cloud water.

The precipitation forecast for the three cases using the Athens model area (frame 2 in Fig. 2) are shown in Fig. 8. Precipitation forecast maps are shown for 0000 UTC 6 March 2005. The LM-z forecast is less noisy than that of the LM-tf, showing fewer maxima. For example, in the northeast of Greece, north of 42.5° and east of 25°E there are seven precipitation maxima with LM-tf and only three with LM-z. In spite of being

→

FIG. 8. Twelve-hour precipitation forecasts for the Athens model version. (top left) Precipitation forecast (mm) for LM-tf verifying (1800–0600 UTC) 0600 Mar 2005. (top right) As in left, but for LM-z. (bottom) The number of synoptic station verifications for the 1800–0600 UTC precipitation and three initial dates of forecasts. Red indicates the number of stations where LM-tf performs better and blue the number of stations where LM-z is better. Yellow indicates the number of stations where no precipitation was observed and none of the LM-model versions forecasted rain. (middle) Graphic visualizations of the observed 1800–0600 UTC precipitation (mm) for all Greek SYNOP stations (yellow) along with forecasts of LM-tf (red) and LM-z (blue). The initial dates are (top to bottom) 0000 UTC 6 Mar, 0000 UTC 7 Mar, and 0000 UTC 8 Mar 2005.

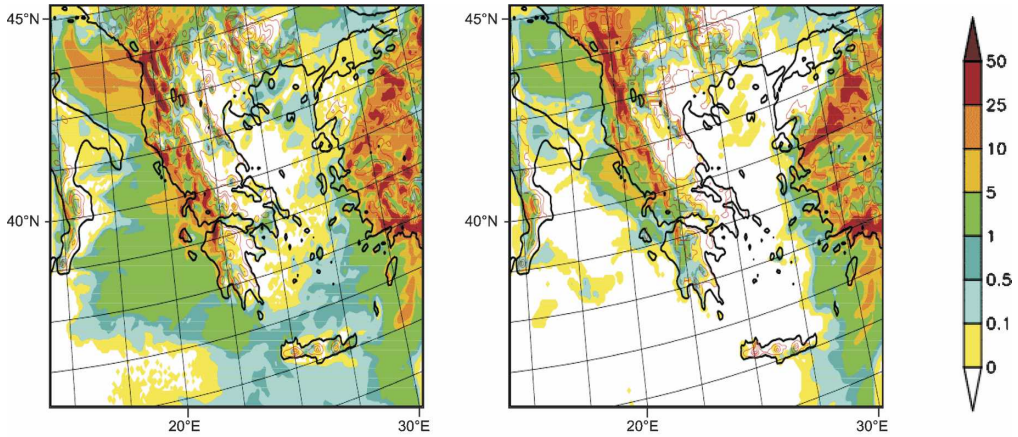
45°N
40°N
20°E
30°E
45°N
40°N
20°E
30°E
50
25
10
5
1
0.5
0.1
0

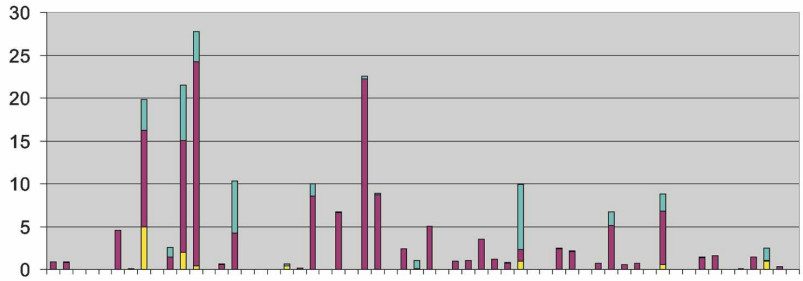
30
25
20
15
10
5
0

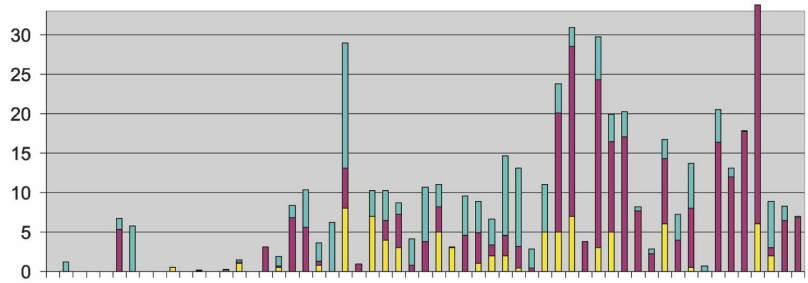
30
25
20
15
10
5
0

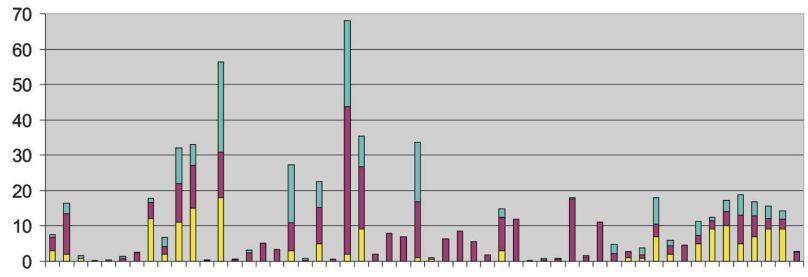
70
60
50
40
30
20
10
0

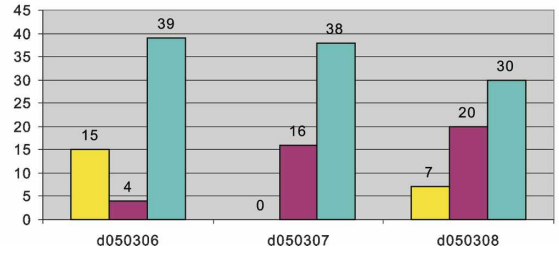
45
40
35
30
25
20
15
10
5
0
15
4
39
0
16
38
7
20
30
d050306
d050307
d050308

smoother, the LM-z forecast often has more pronounced mesoscale structures, such as the precipitation band in the north of Turkey. It is stronger with LM-z and more separated from the rain in the south. The large area of light rain over the sea with the LM-tf is substantially reduced with LM-z. This phenomenon of extended drizzle is common to many models and is known as "socialist rain." At least for the sea area west of Greece the dry forecast of LM-z seems to be better, as the IR satellite images (figure not shown) show no clouds there.

The 24-h precipitation measurements from the surface synoptic observations (SYNOP) net are used to evaluate the forecasts. The SYNOP stations in Greece and Turkey are too few to allow good analyzed precipitation maps. The stations tend to be in coastal areas, where for this particular case strong gradients in the precipitation pattern make a visual verification from observations plotted into maps difficult. Therefore a station-to-station verification is used. A graphic illustration of all Greek synoptic stations and the corresponding forecasts of LM-tf and LM-z is given in the three middle panels of Fig. 8. The observations are indicated in yellow, the forecasts by LM-z in blue, and those of LM-tf in red. On average, the LM-z gives the better QPF for all three cases. In particular, the LM-tf quite often overpredicts the precipitation by a large amount. This was a known problem for forecasters using the LM-tf at the time when this version of LM-tf was operational (H. Kurz, DWD, 2001, personal communication). The LM-z forecasts have a more realistic range. The LM-z prediction is not always lower than that of the LM-tf. In some places the LM-z predicts rain when the LM-tf does not. The advantage of the LM-z over LM-tf came mostly from situations when it avoided the strong overprediction produced by LM-tf. The cases where LM-z produced more rain than LM-tf were worse in a number of cases, but not always. For example the second observation from right for the 0000 UTC 6 March 2005 case rightly predicts rain when the LM-tf does not. The bottom panel of Fig. 8 shows the number of stations where LM-z was better (blue) and those where LM-tf was better (red). The yellow bar in this diagram indicates the number of stations where no precipitation was observed and both models predicted no precipitation. For all three cases in the Athens model area the LM-z was better than LM-tf at a larger number of stations.

The LM-z discretization differs from that of LM-tf not only in the immediate vicinity of orography. Clouds over the sea in the Athens model version are to the windward side of mountains. The upwind areas forecasted with the LM-tf extend several hundred kilometers to windward. Therefore a substantial impact of the z discretization over the sea is not surprising. This point will be investigated further using a case with the Rome model area with initial date 0000 UTC 29 April 2005.

This case is characterized by the passage of a warm and a cold front over France. These fronts are occluding later in the forecast. Because of high pressure in the Alpine area there is little wind in the Alps and northern Italy during this time, both at the surface and at 500 hPa. The vertical velocities w at height 5000 m and forecast time 12 h are shown in Fig. 9 for the two forecasts using LM-tf (top) and LM-z (bottom). The color code was chosen to distinguish the smaller values of w between -6 and 6 cm s^{-1} even though both forecasts reach values above 1 m s^{-1}. The striking difference between the forecasts is that the area of large vertical velocities is considerably reduced with LM-z. For this particular case both the LM-tf and the LM-z forecast large w over the mountainous areas of Spain. This area of strong w extends to the adjacent regions of the Mediterranean toward North Africa for several hundred kilometers with both models. This area of enhanced vertical velocities over the Mediterranean is in the lee of the Spanish mountains. Other sea areas, such as the Bay of Biscay and the Mediterranean west of Italy, have much smaller vertical velocities with both model versions. The Bay of Biscay has a large-scale flow approximately parallel to the Spanish mountains and the area west of Italy shows only weak large-scale winds. As opposed to the LM-tf, the LM-z does not show strong vertical velocities over all mountainous areas. The Alps and the Appennine induce small vertical velocities in LM-z. These are again areas of weak large-scale wind and this difference between the two model versions is consistent with the differences observed in the idealized cases, as reported in section 3. Also, the regions of lower mountains in France and Germany have no large vertical velocities with the LM-z. For these areas the LM-tf produces strong w. Therefore, the bands of positive and negative vertical velocities associated with the frontal passage are more visible with LM-z. These bands are sharper and smoother in the LM-z. When looking at these frontal vertical velocity bands at different times, they keep their identity better in the LM-z, resulting in a precipitation pattern evolving more smoothly. Figure 9 also shows w at height 5000 m along the line indicated in Fig. 3, being perpendicular to the front. Here w is given as a function of space and time for LM-tf (top) and LM-z (bottom). The vertical velocities associated with the front are more uniform with LM-z. The feature at grid point 50 interrupting the movement of the frontal passage with LM-tf is caused by a steep valley in the orography having an average

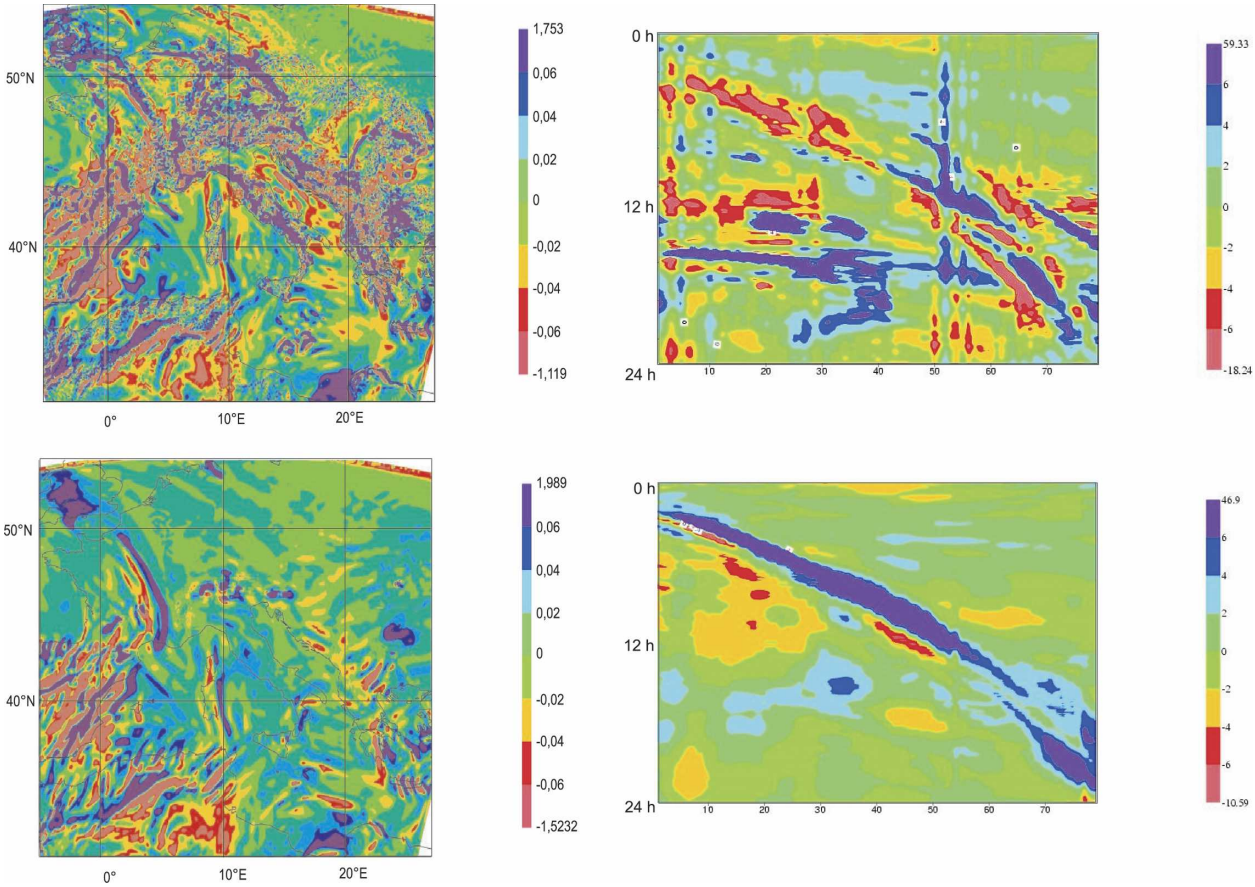

FIG. 9. Twelve-hour forecasts of vertical velocity w in m s^{-1} at a height of 5000 m for (top left) LM-tf and (bottom left) LM-z. The initial date is 0000 UTC 29 Mar 2005. (top right) Forecasted w at a height of 5000 m on a line shown in Fig. 3 as a function of time with LM-tf. The vertical axis gives time in h; the horizontal labels are distances to the southwest end of the line in multiples of 7 km. (bottom right) As in top right, but for LM-z.

height of about 200 m. These strong differences in vertical velocity can be expected to have an impact on the precipitation forecast.

The improvement of QPF in the LM-z is better seen when considering short time intervals. Figure 10 gives the 6-h precipitation forecasts for the LM-tf and the LM-z in 6-h intervals for a section of the forecast area indicated in Fig. 3. This area extends from the Pyrenees to the south of England and includes the Bay of Biscay. This is the area affected by the frontal system. The LM-z shows the warm front as a smoothly moving rainband with moderate precipitation for all four time windows. For the LM-tf this band is broken up into many maxima and minima and has the precipitation varying in time, with most of the frontal precipitation delivered around the forecast time 12 h. The precipitation pattern produced by LM-z is better supported by the observations. The observed rain in Fig. 10 was hand analyzed from SYNOP observations. The white color is used when there is no observation and when the precipitation is zero. Therefore it is possible that for the observations the rainband seems interrupted when in reality there is only a lack of observations. For example the rainy areas predicted with LM-z over southern England and France are connected and appear disconnected in the analyzed observations. However, this difference just reflects a lack of observations over the English Channel. In the 0–6-h forecast interval the trace of a convectional cell that is associated with the passage of the cold front is forecasted with both model versions in the south of the Bay of Biscay, just north of Spain. It is more sharply defined with the LM-z. In the 6–12-h interval this cell enters the land in an area of smaller mountains just north of the Pyrenees. For the LM-z the cell remains sharply defined and happens to pass a station showing an increased precipitation compared with the surrounding stations. For the LM-tf after landfall it splits into three strong precipitation areas. The resulting rather large area of strong precipitation is not supported by the observations.

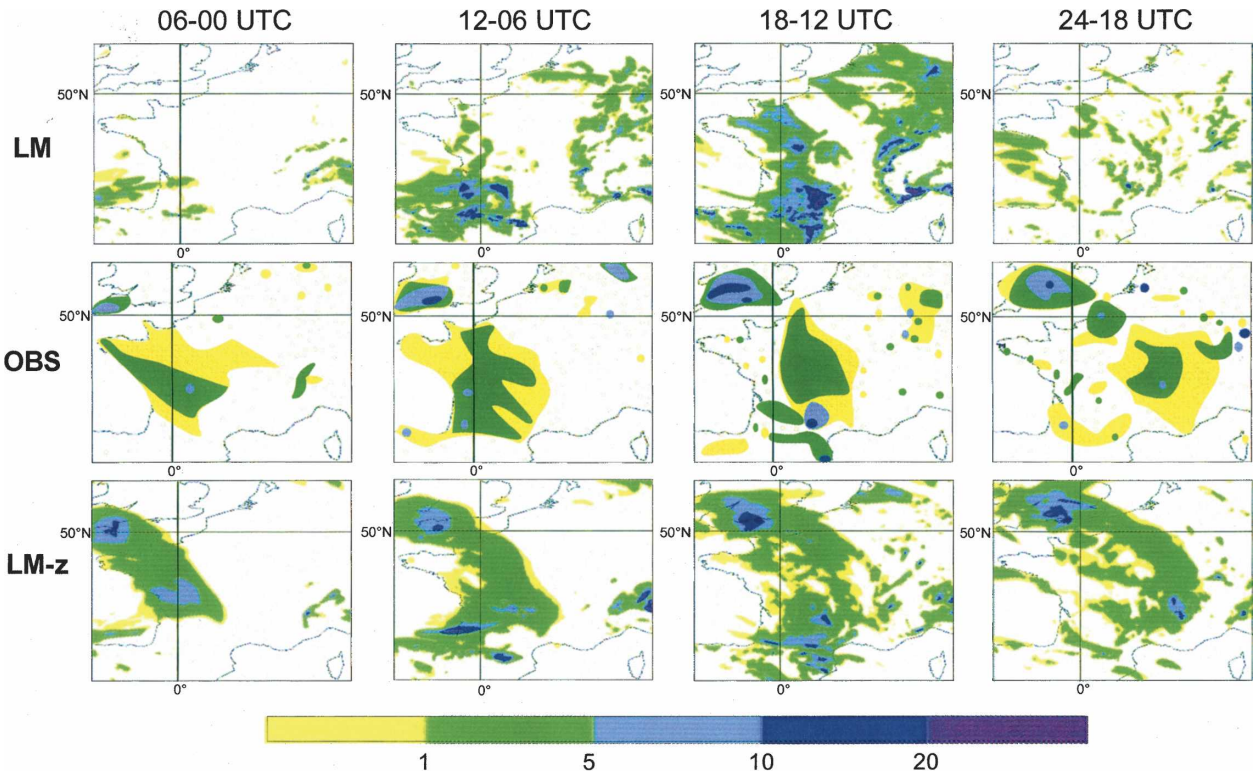

FIG. 10. Accumulated 6-h precipitation forecasts (mm) for initial date 0000 UTC 29 March 2005 for different times and forecasts with (top) LM-tf, (bottom) LM-z, and (middle) observations. The selected area is indicated in Fig. 3.

As the step-mountain concept has the problem of forecasting too-weak winds in the lee of mountains, the example of the flow at a lee coast is investigated to show that the LM-z does not have a similar problem. Figure 11 shows wind forecasts in the south of Italy for the LM-tf and the LM-z for the 24-h forecast starting from 0000 UTC 29 April 2005. The wind speed in meters per second is indicated by the shading. There are four lee wind systems with increased wind speed indicated by both forecasts in the sea area to the southeast and south of the southernmost tip of the Italian mainland. With the LM-z these areas are more pronounced and of slightly higher amplitude than with the LM-tf. Therefore in this case there is no indication of a weakening of lee wind systems by the LM-z. There are not a sufficient number of synoptic stations to verify these mesoscale features. One of the stations is on the land side of one of the enhanced wind areas. The enhanced wind in the Street of Messina is known to seamen since antiquity. This is in accordance with idealized calculations and can be attributed to the use of c1 functions for the representation of mountains, rather than functions of type c0 (see discussion in the introduction).

5. Conclusions

Two versions of the nonhydrostatic model LM were compared. The LM-z uses the z coordinate and the LM-tf a terrain-following coordinate. The forecasts of precipitation produced by these two model versions were very different. The structure of the predicted precipitation was generally better with the LM-z. The quality of QPF was investigated using a total of 39 cases, 1 corresponding to the Warsaw model area, 3 for the Athens, and 35 for the Rome model areas. The threat score for precipitation was substantially higher for the LM-z forecasts. There was also a reduction of RMSE of temperature and vector winds for verifications of the 24-h forecasts against radiosondes. These findings are in agreement with theoretical expectations concerning the advantages of a z-coordinate model and with the results of idealized test integrations. The LM-z is developed further toward operational use in a special project of the Consortium for Small-Scale Modeling (COSMO). For further research into the LM-z there is the planned European Union project Very High Resolution Environmental Workshop (VHREM; http://www.env.leeds.ac.uk/~alan/vhrem) coordinated by A. Gadian. VHREM aims at creating numerical proce-

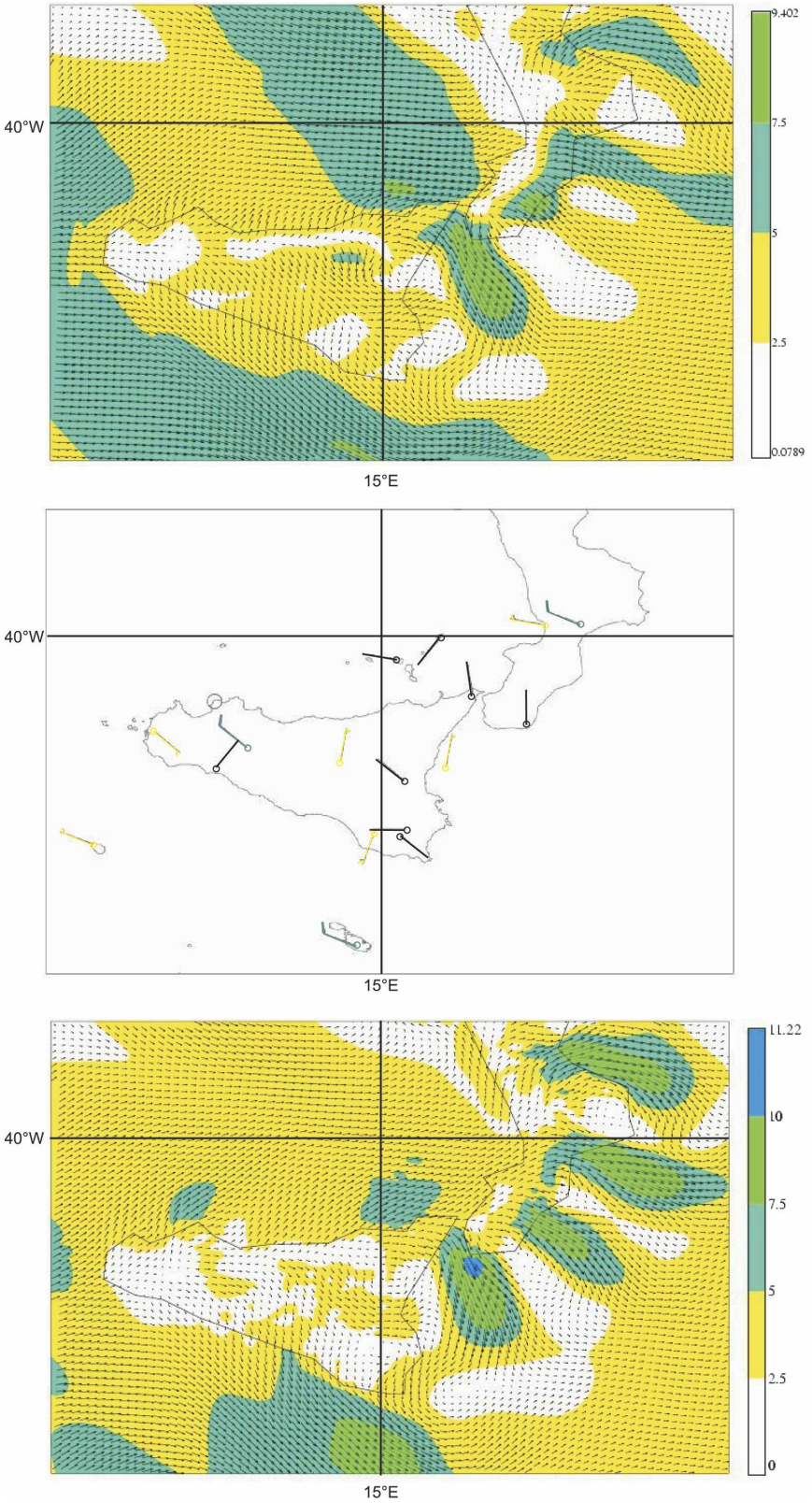

FIG. 11. Twenty-four-hour wind forecasts and verifying observations for an area in the south of Italy showing mesoscale lee wind effects for (top) LM-tf; (bottom) LM-*z*; (middle) verifying observations. The initial date is 0000 UTC 29 Mar 2005. The shading indicates the wind speed ($m\ s^{-1}$). The black wind barbs correspond to the white color in the shading.

dures for next-generation models. The smaller project meso-flow-LM dealing just with LM-z is planned with DFG.

Acknowledgments. The work reported profited from a four-week visit of Z. Janjic to DWD, which was made possible through cooperation between NCEP and DWD and was financed by DWD. The technical assistance for the graphics by Yvonne Schmidt-Reiter is gratefully acknowledged.

APPENDIX

Grid Options Avoiding the Interpolation Error of the Physics Interface

As described in section 2, the physics interface involves two grids. This has potential disadvantages as the interpolation error of the physics interface may have an undesirable impact on the solutions. In particular, there may be the danger of separation of solutions on the two grids. As in this paper only short-range forecasts of up to 30 h were done; no special procedure was used to keep the solutions together. In a related approach by Molod (2005, manuscript submitted to *Mon. Wea. Rev.*, hereafter MOL) intended for longer integrations, a numerical procedure to keep the solutions together was proposed. The aim of this appendix is to define grids where the procedure outlined in section 2 is equivalent to using only one grid and to define projection procedures I avoiding the interpolation error altogether. This is achieved by choosing the refined physics grid to be an extension of the coarser z grid.

Let us define model levels to be those where all fields except w are defined. The half levels are those in between the model levels. In the LM w is not used for physics and therefore all fields being transformed by the operators I and I^{-1} are defined on model levels. Let the z grid be given. Two methods of grid refinement to obtain the physics grid are considered. The model-level method adds model levels to the z grid and the half-level method adds half levels to the z grid.

For refined grids of this kind we can consider the z grid as part of the physics grid. The operator I of section 2 is given by linear interpolation for the model-level method. For the half-level method the operator I extends the same z-level amplitude to all physics level amplitudes whose half-level intervals are contained in the z-layer's half-level interval. The operator I^{-1} is defined by choosing for the model-level method the amplitudes corresponding to the z grid (being part of the physics grid). For the half-level method the coarse-mesh amplitudes corresponding to the z grid are obtained by averaging the physics-level amplitudes being contained in its grid interval. As now the z grid is a subgrid of the physics grid, the operators I and I^{-1} are identical on the z grid.

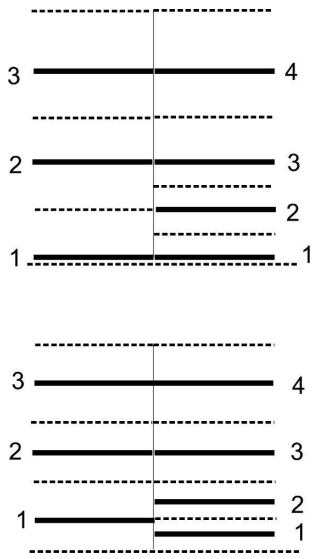

FIG. A1. The (left) z grid and (right) physics grid for the (top) full-level method and (bottom) half-level method. The model levels are indicated as solid lines, and the half levels dashed. The model levels are numbered starting from the bottom.

For illustration, consider the simple example where the z grid has just three model levels, shown as solid lines in Fig. A1. The full-level method is shown on top, and the half-level method on the bottom. The z grid is shown to the left and the physics grid to the right. The half-level z grid then has four levels, the lowest being identical with the earth surface and the top indicating the top of the model atmosphere. For the full-level method (top of Fig. A1), it is convenient to choose the lowest full level just above the earth surface. Consider the example that one level near the surface is added to obtain the physics grid. In realistic models it is normally desired to have an irregular refinement of the lowest level. Here for simplicity we consider the example that the lowest level is just split into equal parts. For the full-level method the new full level is chosen in the middle of z levels 1 and 2. The lowest physics grid full level is then identical to the lowest z-grid level. Except for the newly introduced level, the interpolation to the physics grid amounts to a renumbering and therefore will not result in an interpolation error. The half-level method introduces a new half level in the middle between the lowest two half levels. The lowest full level of the z grid is then divided into two full levels of the physics grid. For both methods the upper levels of the p grid are obtained from the z grid just by renumbering. The transformation equations for the operator I from the z to the physics grid for a field g are then for the full

level method: $g_1^p = g_1^z$; $g_2^p = (g_1^z + g_2^z)/2$; $g_3^p = g_2^z$; $g_4^p = g_3^z$. For the half-level method, shown in the bottom of Fig. A1, the corresponding equations are $g_1^p = g_1^z$; $g_2^p = g_1^z$; $g_3^p = g_2^z$; $g_4^p = g_3^z$. For the transformation I^{-1} from the p to the z grid we obtain for the full-level method: $g_1^z = g_1^p$; $g_2^z = g_3^p$; $g_3^z = g_4^p$, and for the half-level method: $g_1^z = (g_1^p + g_2^p)/2$; $g_2^z = g_3^p$; $g_3^z = g_4^p$. In these equations the values on the right-hand side are considered to be given and the left-hand side is defined.

The mathematically inclined reader may consider the discretization space of the physics grid as the function space spanned by the linear interpolating functions for the model-level method. For the half-level method the discretization space is generated by the functions being piecewise constant on half level intervals. The z-grid subspaces are then the spaces generated by the functions corresponding to the z levels only.

The physics interface described in section 2 can now be seen to work on the physics grid, from which the z-grid can be generated at every time step. The physics time step is performed every time step in the normal way and the dynamics step is performed on the z subgrid and the tendencies are transformed to the physics grid using the operator I.

Both the model-level and the half-level methods allow the development of finescale structures forced by the physics routines even when the z grid is too coarse to support them. The model-level method will create such structures by precipitation and boundary layer processes. The half-level method will create no finer scales by precipitation processes, but only by the other physics processes.

A similar method, defining the z grid as a subgrid of the physics grid, was used by MOL. As MOL defined the operator I by averaging when using the model-level method, an interpolation error was encountered and measures had to be taken against grid separation despite using a suitable grid.

REFERENCES

Bryan, K., 1969: A numerical method for the study of the circulation of the World Ocean. *J. Comput. Phys.,* **4,** 347–376.

Gallus, W. A., Jr., 2000: The impact of step orography on flow in the Eta Model: Two contrasting examples. *Wea. Forecasting,* **15,** 630–637.

——, and J. Klemp, 2000: Behavior of flow over step orography. *Mon. Wea. Rev.,* **128,** 1153–1164.

Janjic, Z. I., 1977: Pressure gradient force and advection scheme used for forecasting with steep and small scale topography. *Contrib. Atmos. Phys.,* **50,** 186–199.

Kröner, D., 1997: *Numerical Schemes for Conservation Laws.* Wiley & Sons, 505 pp.

Mesinger, F., Z. Janjic, S. Nicovic, D. Gavrilov, and D. Deaven, 1988: The step-mountain coordinate: Model description and performance for cases of Alpine lee cyclogenesis and for a case of Appalachian redevelopment. *Mon. Wea. Rev.,* **116,** 1493–1518.

Pielke, R. A., and M. Segal, 1986: Mesoscale circulations forced by differential terrain heating. *Mesoscale Meteorology and Forecasting,* P. S. Ray, Ed., Amer. Meteor. Soc., 516–548.

Saito, K., G. Doms, U. Schättler, and J. Steppeler, 1998: 3-d mountain waves by the Lokal Modell of DWD and the MRI Mesoscale Nonhydrostatic Model. *Pap. Meteor. Geophys.,* **49,** 7–19.

——, J. Steppeler, T. Kato, H. Eito, N. Seino, and A. Murata, 2001: Meeting summary: Report on the Third International SRNWP (Short Range Numerical Weather Prediction) Workshop on Nonhydrostatic Modelling. *Bull. Amer. Meteor. Soc.,* **82,** 2245–2250.

Staudenmaier, M. J., and J. Mittelstadt, 1997: Results of the western region evaluation of the Eta-10 model. Western Region Tech. Attachment 97-18, 12 pp. [Available from National Weather Service Western Region-SSD, 125 S. State St., Rm. 1311, Salt Lake City, UT 84147.]

Steppeler, J., H. W. Bitzer, M. Minotte, and L. Bonaventura, 2002a: Nonhydrostatic atmospheric modelling using a z-coordinate representation. *Mon. Wea. Rev.,* **130,** 2143–2149.

——, U. Schättler, H. W. Bitzer, A. Gassmann, U. Damrath, and G. Gregoric, 2002b: Meso gamma scale forecasts by nonhydrostatic model LM. *Meteor. Atmos. Phys.,* **82,** 75–96.

Sundqvist, H., 1976: On vertical interpolation and truncation in connection with the use of sigma system models. *Atmosphere,* **14,** 37–52.

Wallace, J. M., S. Tibaldi, and A. J. Simmons, 1983: Reduction of systematic forecast errors in the ECMWF model through the introduction of an envelope orography. *Quart. J. Roy. Meteor. Soc.,* **109,** 683–717.

Zängl, G., 2002: An improved method for computing horizontal diffusion in a sigma-coordinate model and its application to simulations over mountainous topography. *Mon. Wea. Rev.,* **130,** 1423–1432.